Received March 25, 2021, accepted April 28, 2021, date of publication May 10, 2021, date of current version May 18, 2021.

Digital Object Identifier 10.1109/ACCESS.2021.3078534

Complementary Photoplethysmogram Synthesis From Electrocardiogram Using Generative Adversarial Network

HEEAN SHIN[1], SUKKYU SUN[2], JOONNYONG LEE[3], AND HEE CHAN KIM[1,4,5], (Member, IEEE)

[1]Interdisciplinary Program in Bioengineering, Graduate School, Seoul National University, Seoul 08826, Republic of Korea
[2]Biomedical Research Institute, Seoul National University Hospital, Seoul 03080, Republic of Korea
[3]Mellowing Factory Company Ltd., Seoul 06053, Republic of Korea
[4]Institute of Medical and Biological Engineering, Medical Research Center, Seoul National University, Seoul 08826, Republic of Korea
[5]Department of Biomedical Engineering, Seoul National University College of Medicine, Seoul 03080, Republic of Korea

Corresponding authors: Joonnyong Lee (joonnyonglee@melab.snu.ac.kr) and Hee Chan Kim (hckim@snu.ac.kr)

This work was supported by the Bio and Medical Technology Development Program of the National Research Foundation (NRF) funded by the Korean Government (MSIT) under Grant 2016M3A9F1939646.

ABSTRACT Photoplethysmogram (PPG) is one of the most widely measured biosignals alongside electrocardiogram (ECG). Due to the simplicity of measurement and the advent of wearable devices, there have been growing interest in using PPG for a variety of healthcare applications such as cardiac function estimation. However, unlike ECG, there are not many large databases available for clinically significant analyses of PPG. To overcome this issue, a Generative Adversarial Network-based model to generate PPG using ECG as input is proposed. The network was trained using a large open database of biosignals measured from surgical patients and was externally validated using an alternative database sourced from another hospital. The generated PPG was compared with the reference PPG using percent root mean square difference (PRD) and Pearson correlation coefficient to evaluate the morphological similarity. Additionally, heart rate measured from the reference ECG, reference PPG, and generated PPG, and compared through repeated measure analysis of variance to test for any significant differences. The mean PRD was 32±10% and the mean correlation coefficient was 0.95±0.05 in the test dataset. The HR from the three biosignals showed no significant difference with a p-value of 0.473. When the optimized GAN model was tested on atrial fibrillation ECG from a third dataset, the mean correlation coefficient between the generated PPG heart rate and the ECG heart rate was 0.94±0.15, with paired t-test resulting in p-value of 0.64. The results indicate that the proposed method may provide a valuable alternative to augmenting biosignal databases that are abundant in one signal while lacking in another.

INDEX TERMS Data augmentation, deep learning, electrocardiogram, generative adversarial networks, photoplethysmogram.

I. INTRODUCTION

Photoplethysmogram (PPG) is a blood pulse signal measured using light reflection or transmission, which amplitude and morphology are dependent on the blood volume and vascularity of the measured tissue. PPG is used in various systems ranging from smartphones to pulse oximeters, and has recently become more ubiquitous due to the expansion of the wearable devices industry [1]–[4] and growing number of healthcare applications in cardiovascular monitoring [5]–[7]. In conjunction with the explosion in deep neural network based biosignal processing techniques, recent studies have shown promising results on cardiac function analyses using PPG [8]–[10].

Since 2016, studies on blood pressure estimation [9], [11], [12], biometric identification [13], [14], and atrial fibrillation detection [15]–[18] from PPG signals using deep learning has become popular. Some of these studies were able to use readily available public databases for training the deep learning models [19]–[21], but others required conducting large-scale experiments to produce the necessary data [15], [22], [23]. Because deep learning models need large datasets for proper optimization, the availability of data in large quantities becomes a limiting factor in developing such methods, as generating properly annotated databases require vast resources which can be afforded by a few. Even when the

The associate editor coordinating the review of this manuscript and approving it for publication was Sunil Karamchandani.

necessary data is present, accessing it for research purposes can be difficult since the institutions which own the database may refuse opening health data citing privacy concerns [24].

The development of electrocardiogram (ECG)-based deep learning methods for cardiovascular health monitoring have been much more widespread due to the number of easily accessible public ECG databases with cardiologist annotations for various conditions [25]. Adapting these annotations into synchronized PPG could be beneficial in increasing such research using PPG instead of ECG, but unfortunately, most annotated ECG databases do not have simultaneously measured PPG. There have been attempts to generate PPG, which could potentially turn these annotated ECG databases into useful sources for generating annotated PPG data. In [26], A. Solosenko *et al*. generated synthetic PPG signals using linear combinations of a log-normal and Gaussian waveforms. With the advance of deep learning techniques, especially of generative adversarial network (GAN), generation of time series biosignal data using GAN have been recently investigated [27]–[32]. In a recent study of ECG generation among these studies [31], ECG simulator information was used to enhance the performance of the GAN model by augmenting Euler loss to the general cross-entropy loss. In [32], a bidirectional grid long short term memory based generator with convolutional neural network (CNN) based discriminator were used to generate four kinds of biosignals including ECG and PPG. Regarding PPG generation, [29] used GAN to synthesize PPG data from random seeds, but the authors acknowledged that the generated signal included high frequency components which required significant post-processing before the signal resembled high-quality PPG. However, none of these studies have used ECG as a source to generate PPG, and the resulting synthetic PPG data have been bound to the design of the generation model.

In this paper, a novel method to generate PPG from ECG recording using GAN is introduced. First, the GAN architecture is described in detail along with the training dataset in the Methods section. In the Results section, synthetic PPG generated using ECG is compared against simultaneously measured PPG using validation data and testing data from an alternative dataset. Then, synthetic PPG is analyzed in terms of morphological and physiological metrics, and the value of the proposed method is discussed in relation to synthetic atrial fibrillation PPG dataset generation in the Discussions section.

By validating the GAN-generated PPG in terms of error, correlation, and atrial fibrillation, this study demonstrates that GAN can be a potential tool to generate synthetic biosignals for data augmentation purposes in low resource settings.

II. MATERIALS AND METHODS

A. RELATED WORKS IN GAN-BASED BIOSIGNAL GENERATION

Since its proposal in 2014 [33], GAN has been developed for diverse applications ranging from language processing to image generation. GAN is composed of a generator network which produces a desired output, and a discriminator network which determines if its input is real or artificial. As the generator outputs some synthetic data, these are fed into the discriminator along with real data, and the discriminator is trained to distinguish between the real and fake data, while the generator is trained to produce synthetic data that are closer in form to the real data. It is probably the best-known for image style transfer methods [34], which transcribes the artistic style of one image to another image, popularized by many smartphone camera applications, however, it has been applied to biosignals in a few cases, especially for data augmentation purposes. In one study, recurrent neural network (RNN)-based generator was used along with a CNN-based discriminator to generate artificial ECG that are indistinguishable from measured ECG [27]. In another study, GAN was used to generate a synthetic PPG dataset in order to augment a pre-existing database without unwanted byproducts of traditional data augmentation methods such as time-warping and additional noise [35]. Other studies have generated non-periodic medical data such as heart rate, oxygen saturation, and respiratory rate using GAN [36]. On examination, all of these methods have in common that during synthetic data generation after GAN optimization, inputs to the generator were chosen at random following Gaussian distribution, suggesting that there isn't an explicit relationship between generator input and output. In this work unlike in previous studies, GAN was used to generate PPG using ECG as the input to the generator. The discriminator was trained to distinguish between generated PPG and real PPG measured simultaneously with the input ECG.

B. TRAINING DATABASE

Public biosignal data from 6388 patients undergoing various surgeries at Seoul National University Hospital (VitalDB) were used for this study [37]. Lead II ECG and simultaneously measured PPG were recorded at 500Hz on a commercial patient monitor (Tram-Rac4A). For the purposes of this study, the signals were downsampled to 100Hz. On average, each recording was 93 minutes long, but only regions with valid signal range were selected for further processing. As seen on Fig. 1, recordings without both ECG and PPG were excluded. Then, largest continuous durations without saturation or missing values was selected for each recording, and 60-second segments of ECG and PPG from these regions were extracted with 57-second overlap. To compensate for the varying delays between ECG and PPG, for each ECG segment, corresponding 60-second PPG segment was found by considering 60-second PPG segments from the same period plus 3 seconds with PPG HR and ECG HR correlation above 0.96. For example, if a particular segment of ECG was extracted between 1000 to 1060 seconds of a given recording, the corresponding 60-second PPG segment was found between 1000 to 1063 seconds of the recording based on the correlation between the HR of the extracted ECG segment and the HR of the PPG segment candidates which lie between 1000 to 1060 seconds, 1000.01 to 1060.01 seconds, and etc.

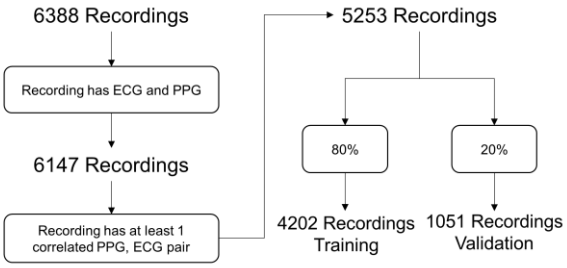

FIGURE 1. Block diagram of the data selection process from the VitalDB database. Out of 6388 patient recordings, a total of 5253 recordings were used to optimize GAN model. [Note: ECG, electrocardiogram; PPG, photoplethysmogram; GAN, generative adversarial network].

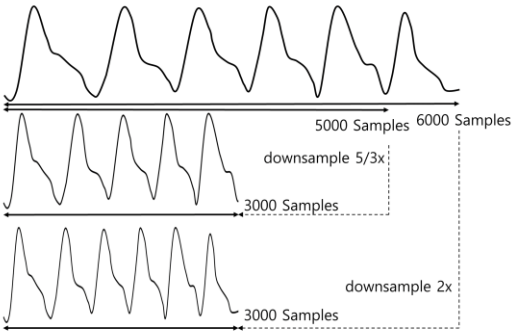

FIGURE 2. Figure of the downsampling process used to achieve high variation in heart rate in the training data.

Recordings without highly-correlated (i.e. correlation above 0.96) ECG-PPG pairs were excluded, and the remaining recordings were separated in 4-to-1 ratio for GAN training and validation. Afterwards, 60-second segments were randomly downsampled by a factor between 1 to 2 in order to adjust for low variations in heart rate in surgery patient data as shown in Fig. 2. ECG-PPG pairs were further segmented into 0.5, 1, 1.25, 1.5, and 2 second fragments for training the GAN at various signal lengths. However, only 1-second fragments were used for external validation due to the lowest loss values following optimization (Fig. 3). 200 segments were selected at random from each record, normalized in magnitude, and saved for GAN optimization.

C. PROPOSED GAN ARCHITECTURE

The architecture of the proposed GAN is shown in Fig. 4. 1-second length (100 samples) ECG fragments was fed into a RNN-based generator composed of one bidirectional Long Short-Term Memory (LSTM) [38] layer with 30 cells activated with Tanh and forget bias value of 1. At each time step, samples of the ECG segment were sequentially inputted into the LSTM layer, and at the last time step, the states of the LSTM cells were fully-connected to an output layer with size equal to the original sample length of the ECG fragment. For

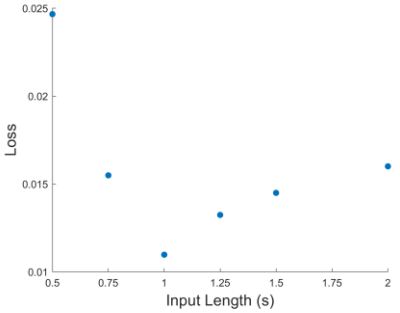

FIGURE 3. The loss values of the GAN following optimization at various input signal lengths.

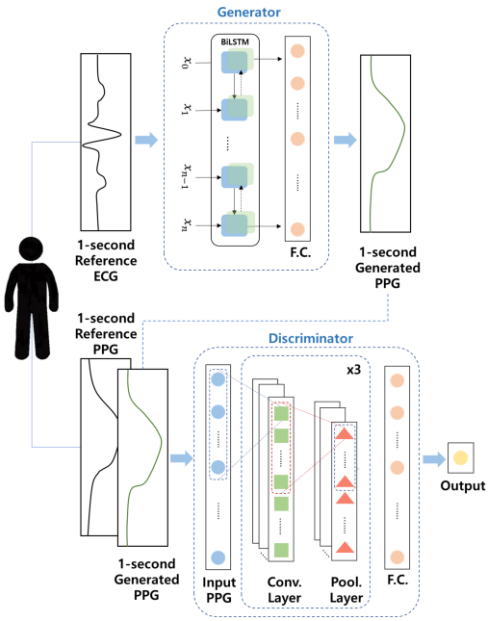

FIGURE 4. Flow diagram for the proposed GAN architecture. The RNN-based generator takes ECG as an input, and outputs generated PPG. The output from the generator is fed into the CNN-based discriminator which is trained to distinguish between synthetic PPG and real PPG. [Note: BiLSTM, bidirectional long short-term memory; ECG, electrocardiogram; PPG, photoplethysmogram; CNN, convolutional neural network; RNN, recurrent neural network; Conv., convolutional; Pool., pooling; F.C., fully-connected].

the kernel initializer of the fully-connected layer, truncated normal initializer with standard deviation of 0.01 was used and all biases were initialized with 1.

The output from the generator was then fed into a CNN-based discriminator network as shown in Fig. 4. The discriminator architecture consists of 3-layer CNN, with 8, 16, 32 filters respectively. Kernel size of 5 was applied to all the convolution filters with stride 1. The kernel weights were initialized using truncated normal initializer with standard deviation of 0.01 and the biases were initialized with 1. Following convolution, the hidden states were activated using ReLu and max-pooled by a factor of 5x. After 3 convolution layers, the output was fully-connected to a dense layer with 32 nodes. This fully-connected layer was initialized in the

same manner as the fully-connected layer in the generator. The output was activated using sigmoid then connected to a single output for the calculation of binary cross entropy loss. Mean-squared error (MSE) loss was calculated between the output of the generator and the reference PPG to improve the quality of signal generation. The pseudocode for the GAN optimization process is shown below:

Algorithm 1 Minibatch Stochastic Gradient Descent Training of Proposed Method

for number of training iteration **do**

- Sample minibatch of m reference ECG $\{ECG^{(1)}, \ldots, ECG^{(m)}\}$
- Sample minibatch of m reference PPG $\{PPG^{(1)}, \ldots, PPG^{(m)}\}$
- Generate m synthetic PPG samples from ECG $\left\{\overline{PPG}^{(1)}, \ldots, \overline{PPG}^{(m)}\right\}$

$$\overline{PPG}^{(i)}_{[1,\ldots n]} = G\left(ECG^{(i)}_{[1,\ldots n]}\right)$$

where n indicates the length of each sample, and $G(x)$ is the differentiable function representing the generator

- Update the discriminator by descending its stochastic gradient:

$$\nabla_{\theta_d} \frac{1}{m} \sum_{i=1}^{m} [-\log\left(D\left(PPG^{(i)}\right)\right) - \log\left(1 - D\left(\overline{PPG}^{(i)}\right)\right)]$$

where $D(x)$ is the output of the discriminator representing the probability that x is from the reference data rather the generator's distribution

- Update the generator by descending its stochastic gradient:

$$\nabla_{\theta_g} \frac{1}{m} \sum_{i=1}^{m} [0.001 \cdot -\log\left(D\left(\overline{PPG}^{(i)}\right)\right) + \frac{1}{n} \sum_{l=1}^{n} (PPG_l^{(i)} - \overline{PPG}_l^{(i)})]$$

end for

Adam optimizer was used.

D. EVALUATION OF THE OPTIMIZED GAN

As shown on Fig. 5, the generator of the optimized GAN was tested using an external dataset from the University of Queensland Vital Signs Database (UQVSD) which also contained simultaneously measured ECG and PPG from 32 patients with median duration 105 minutes [39]. The test dataset was extracted and pre-processed in the same manner as the training dataset, and a total of 1893 30-second segments of data from 27 patients in the database were used for external validation.

To check the morphology of the synthetic PPG, errors between the synthetic PPG and the simultaneously measured PPG were calculated. Percent root mean square difference (PRD), as defined below, was calculated to measure

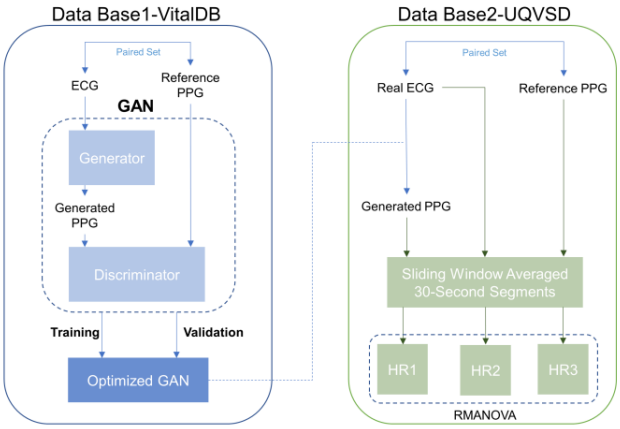

FIGURE 5. GAN training, validation, and testing outline. HR1 is the heart rate calculated from the generated PPG, HR2 is the heart rate calculated from the reference ECG, and HR3 is the heart rate calculated from the reference PPG. [Note: ECG, electrocardiogram; PPG, photoplethysmogram; GAN, generative adversarial network; UQVSD, University of Queensland Vital Signs Database; RMANOVA, repeated measure analysis of variance].

distortion.

$$PRD = \sqrt{\frac{\sum_{n=1}^{N} (X_n - \hat{X}_n)^2}{\sum_{n=1}^{N} (X_n)^2}} \times 100 \quad (1)$$

where $\hat{X}_n$ is n^{th} generated PPG sample, X_n, n^{th} real PPG sample, and N is the total number of samples.

Second, Pearson correlation coefficient was calculated to verify that the synthetic PPG moved in a similar manner to the real PPG, and to quantify the degree of association between the two signals.

$$\rho(A, B) = \frac{cov(A, B)}{\sigma_A \sigma_B} \quad (2)$$

where $cov(A, B)$ is the covariance of A and B, σ_A is the standard deviation of A, and σ_B is the standard deviation of B.

Lastly, in order to verify the synthetic PPG in terms of physiological measures, 30-second PPG segments were generated using the optimized GAN with sliding window averaging (Fig. 6). HR extracted from the synthetic 30-second segments was compared to HR from the counterpart 30-second ECG segments as well as 30-second segments of PPG measured simultaneously with the ECG segments. The HR from these triplets were compared using repeated measure analysis of variance (RMANOVA) test.

III. RESULTS

The discriminator and generator loss of the GAN optimization process for input ECG length of 1 second could be seen on Fig. 7, and an example of a simultaneously measured ECG-PPG pair and the corresponding GAN-generated PPG can be seen on Fig. 8.

The difference between the synthetic PPG produced with the optimized generator and the real PPG from the test dataset resulted in mean PRD of 32.0% and mean Pearson's correlation coefficient of 0.95 as shown in Table1.

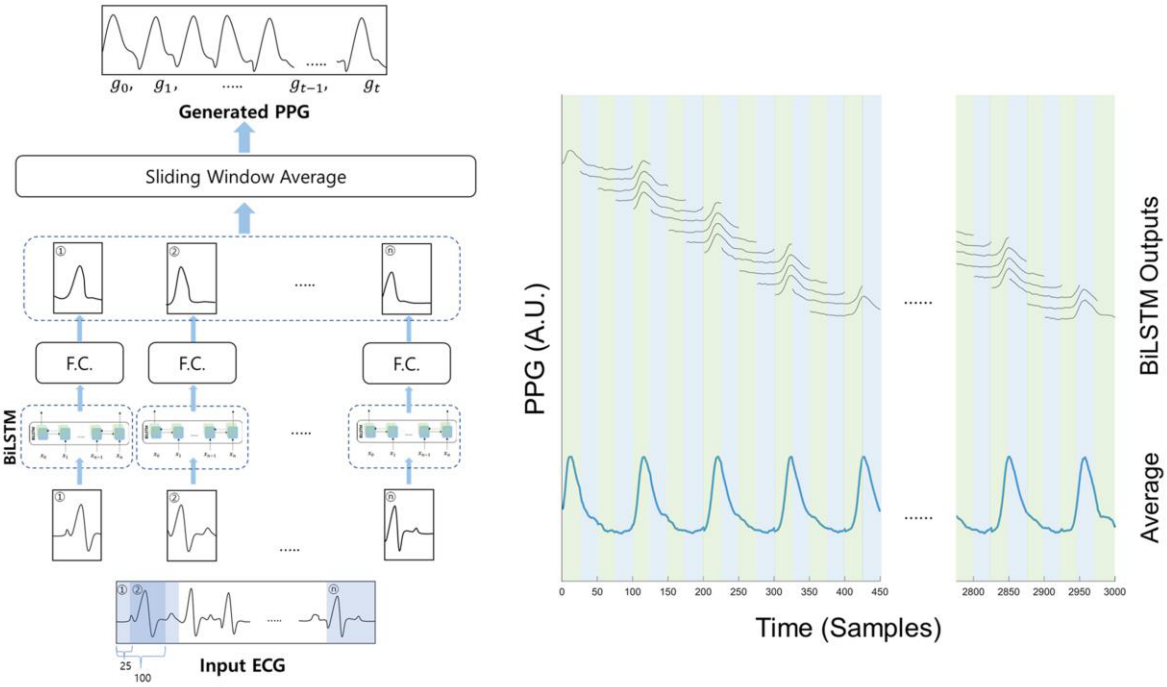

FIGURE 6. a) Diagram representing the generation of 1-second segments of PPG and the subsequent sliding window average for the generation of 30-second PPG segments. 100 samples (1 second) of input ECG data are fed into the optimized BiLSTM network at 25 sample intervals to generate overlapping 100-sample segments of PPG. Then, the overlapping PPG segments are averaged to generate 30-second segments of PPG. The average was multiplied by a factor of four to accentuate the morphology of the generated signal. b) Plot showing the process of averaging 100-sample (1-second) BiLSTM outputs to produce 30-seconds of generated PPG. The shaded regions indicate overlapping four 25-sample BiLSTM outputs averaged to produce the final PPG signal. [Note: ECG, electrocardiogram; PPG, photoplethysmogram; BiLSTM, bidirectional long short-term memory; F.C., fully connected].

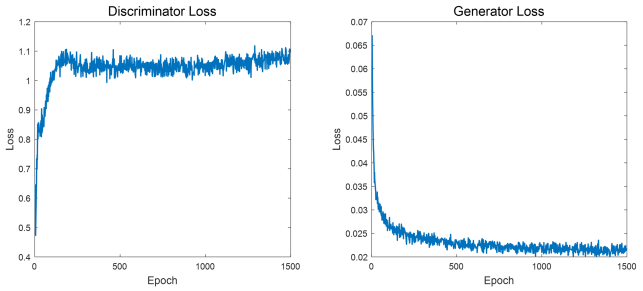

FIGURE 7. Discriminator loss and generator loss of the GAN optimization process. [Note: GAN, generative adversarial network].

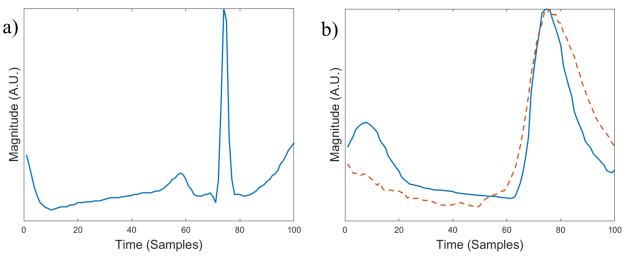

FIGURE 8. a) Reference ECG from University of Queensland Vital Signs Database. b) Reference PPG from University of Queensland Vital Signs Database and PPG generated using ECG on as the input to the optimized GAN (dashed line). [Note: ECG, electrocardiogram; PPG, photoplethysmogram; GAN, generative adversarial network].

The comparison between HR extracted from reference ECG, reference PPG, and synthetic PPG using RMANOVA resulted in a p-value of 0.473, indicating no significant differences.

IV. DISCUSSION

It is challenging to collect sufficient data for developing effective machine learning or deep learning algorithms in the healthcare domain due to privacy concerns as well as costs associated with data acquisition and labeling [40], [41]. These constraints frequently lead to an imbalance in training data distribution [42], resulting in biased algorithms that are impractical for real-world applications. To circumvent these issues, this study proposed a novel GAN-based PPG data augmentation method which can generate low availability data from highly accessible signals, such as ECG.

A. MORPHOLOGY OF THE SYNTHETIC PPG AND POTENTIAL SOURCES OF ERROR

To evaluate the performance of the proposed GAN, PRD and Pearson correlation coefficient were used, as the former is a popular distance measure for quantifying similarity and the latter is a robust measure in quantifying morphological

TABLE 1. PRD & pearson correlation coefficient calculated between reference and synthetic ppg using the test dataset.

Metric	Total Number of Segments	Total Number of Outliers	Mean	STD
PRD (%)	1893	96	31.9	10.3
CC		137	0.949	0.047

[Note: PPG, photoplethysmogram; PRD, percent root mean square difference; CC, correlation coefficient; STD, standard deviation]

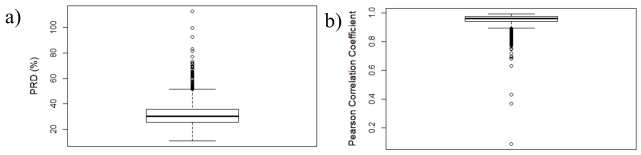

FIGURE 9. Boxplot of PRD (%) and Pearson correlation coefficient of generated PPG from the test dataset. On each box, the middle line indicates the median value, top and bottom edge of the box indicate the 75^{th} and 25^{th} percentiles, respectively. The whiskers of the plot extend to the boundary of the outlier data. The outliers are marked as 'o'. a) Boxplot of PRD (%). b) Boxplot of Pearson correlation coefficient. [Note: PRD, percent root mean square difference].

differences between the synthetic PPG signal and the reference PPG signal. PRD and Pearson correlation coefficient calculated between reference PPG and synthetic PPG using the UQVSD as the test dataset are summarized in Table 1. Corresponding boxplots for these metrics are also shown in Fig. 9. The outliers for each metric (96 segments for PRD and 137 segments for correlation coefficient out of 1893 total, some of which are outliers in both metrics) indicate that some synthesized PPGs are not well-correlated with reference PPGs. Fig. 10 shows pairs of generated PPG segment and the reference PPG from the test dataset with their PRD and Pearson correlation coefficient values. Fig. 10a shows a typical result, which demonstrates that the proposed GAN can generate visually acceptable PPG signals with high correlation and low PRD values.

Fig. 10b and 10c show the resulting PPG pairs for two outliers, which have larger errors. By analyzing these outliers amongst others, it was found that the outliers could be classified into two categories: category I with large PRD and high correlation (as shown in Fig. 10b) and category II with large PRD and low correlation (as shown in Fig. 10c).

In category I, it is likely that the large PRD values are due to dissimilarity in the dicrotic notch between the reference PPG and its synthetic counterpart. As seen in Fig. 10b, dicrotic notch is not visually noticeable in the generated PPG pulse unlike in the reference PPG pulse. The reason behind the dissimilarity may be that the proposed GAN was trained using training dataset collected from patients under anesthesia with mean age of 58±15 years. The dicrotic notch decreases in prominence with aging or vasodilation under anesthesia, which may result in the loss of dicrotic notch in such conditions [43], [44]. Therefore, the PPG pulses belonging to the training dataset may not show a noticeable dicrotic notch as shown in Fig. 11a. However, dicrotic notches are evident in some of the PPG from the testing dataset as shown in Fig. 11b, resulting in high PRD values for the testing data with visible dicrotic notches. Unfortunately, a direct comparison of dicrotic notch prominence between the training and the testing dataset based on age could not be made as the ages of the subjects were not recorded for the UQVSD database, and a further study to validate this incongruity is warranted.

On the other hand, most outliers in category II (as shown in Fig. 10c) seem to arise with rhythmic irregularities within PPG due to arrhythmias such as PVCs (Premature Ventricular Contractions), which results in a large PRD as well as a low correlation value. PVC is not evident in the reference PPG shown in Fig. 10c, but it is evident in the corresponding reference ECG. Fig. 12 shows a more explicit PVC recording in a longer duration of reference ECG and PPG as well as in GAN-generated PPG. In such cases, the proposed GAN does not adequately capture the morphological changes of the PPG signal resulting from PVCs. These findings indicate that the poor performance of the proposed GAN under some specific conditions may be ascribed to the difference in the distributions of physiological conditions between the training dataset and the test dataset. Due to the fact that only 3% of ECG-PPG pairs in the test dataset had PVC recorded, it was not possible to retrain the GAN with sufficient PVC data for better generation of synthetic PPG with PVC. This yields an opportunity for future research in which more data from disease-afflicted individuals could be incorporated into the training process for improving the applicability of the proposed model to a wider range of input data.

B. HEART RATE PRESERVATION IN GENERATED PPG AND POTENTIAL APPLICATIONS TO DATA AUGMENTATION

Analyses of heart rate and heart rate variability (HRV) have broad biomedical applications ranging from diagnosis of cardiovascular diseases based on arrhythmias [45]–[47] to noninvasive assessment of autonomic nervous system (ANS) activities [48]–[52]. Experimental evidences for the association between lethal arrhythmias and sympathovagal imbalance have been reported [53]–[57] and changes in HRV have been associated with derangements in the neural activity of cardiac origin following myocardial infarction [58], [59] as well as with the onset of diabetic neuropathy [60], [61]. Furthermore, a previous work [62] demonstrated that PPG variability (PPGV) could be used as an alternative to HRV by comparing the similarity between PPGV and HRV. With these applications in mind, it is critical to accurately replicate HR and HRV during synthetic PPG generation. In terms of HR, the GAN-generated PPG in the test dataset was statistically indistinguishable to HR measured from the reference ECG and the reference PPG ($p = 0.473$), indicating that the optimized GAN can generate synthetic PPG with HR and HRV similar to the source signal. Therefore, PPG generated using the proposed method may be useful for assessing the

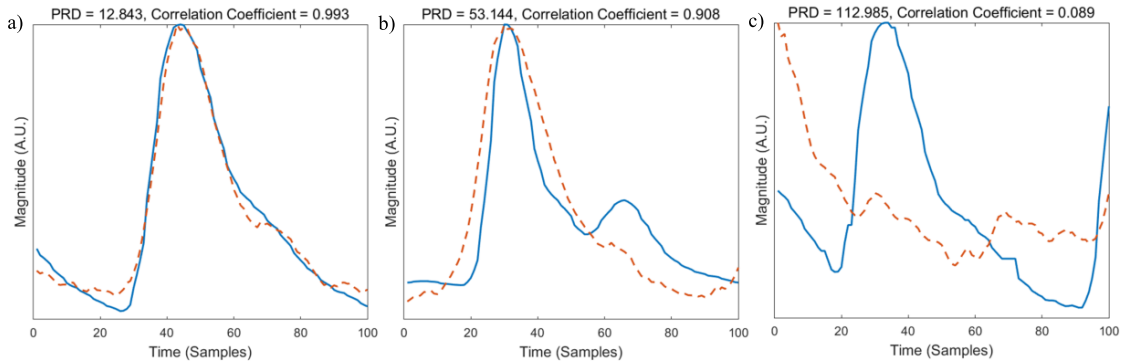

FIGURE 10. a) Generated PPG and reference PPG pair from the test dataset with low PRD and high correlation coefficient. b) Generated PPG and reference PPG pair from the test dataset with high PRD and high correlation coefficient. c) Generated PPG and reference PPG pair from the test dataset with high PRD and low correlation coefficient. PRD value greater than 100% indicates that the difference between the amplitudes of the generated signal and the reference signal is greater than the amplitude of reference signal. Solid lines indicate the reference PPG and dashed lines represent the generated PPG. [Note: ECG, electrocardiogram; PPG, photoplethysmogram; PRD, percent root mean square difference].

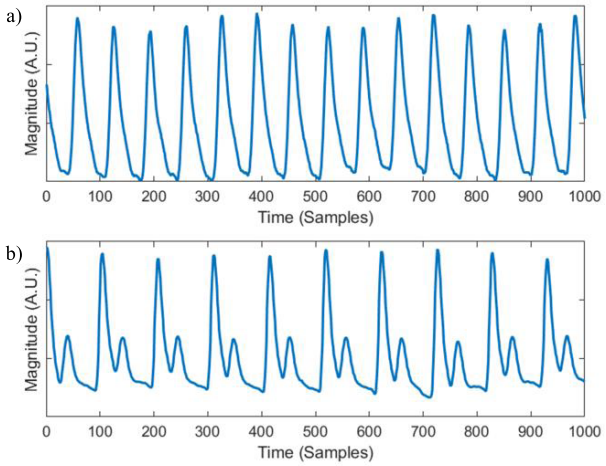

FIGURE 11. a) Training PPG dataset example. As with most of training data, dicrotic notch is not observed. b) Testing PPG dataset example. Dicrotic notches are visible in some of the testing data. [Note: PPG, photoplethysmogram].

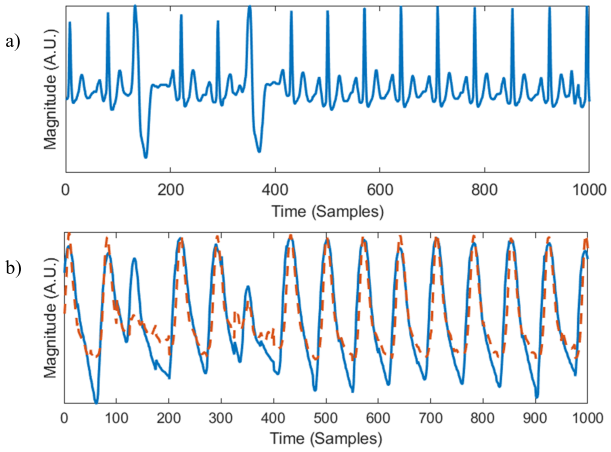

FIGURE 12. a) ECG with PVC in the test dataset. b) Generated and reference PPG corresponding to the above ECG with PVC. Solid line represents the reference PPG and dashed line represents the generated PPG. [Note: ECG, electrocardiogram; PPG, photoplethysmogram; PVC, premature ventricular contraction].

ANS activities in cardiovascular control under various physiological and pathological conditions.

There are many open databases that consist of annotated ECG signals (e.g., MIT-BIH arrhythmia, MIT-BIH atrial fibrillation, etc…). Since ECG is used as the gold standard for diagnosing arrhythmia, for the collection of arrhythmia-annotated PPG, ECG has to be simultaneously measured as well. However, none of the public ECG databases with annotation contain simultaneously measured PPG signals.

In order to develop deep learning-based methods for arrhythmia classification in PPG, a large dataset of annotated PPG is required. Since the proposed model can preserve the heart rate of the source ECG signal, it can be used to generate an annotated PPG database that could be useful for the development of PPG-based arrhythmia classification models.

Atrial fibrillation is one of the most common cardiac arrhythmias [63]–[65]. Atrial fibrillation has been traditionally diagnosed by analyzing rhythmic (i.e. variability of RR intervals) and/or morphological (i.e. absence or irregularity of P-wave) properties of the ECG signal [66]–[69]. It has been recently shown that atrial fibrillation episodes can be detected using features derived from beat-to-beat interval based on PPG signal as an alternative to existing ECG based solutions, where various features (such as the normalized root mean square of successive differences (RMSSD), sample entropy, etc.) from PPG are equivalent to the ones from ECG [70]. Using these insights, numerous studies have employed PPG signals recorded with wearable devices to detect atrial fibrillation episodes [15], [16], [71]–[74]. However, as mentioned previously, these attempts face challenges as there are no atrial fibrillation PPG datasets available for public access.

Thus, to test whether the proposed PPG generation model can be used in one of the predominant arrhythmia conditions, open atrial fibrillation data from Long Term AF Database

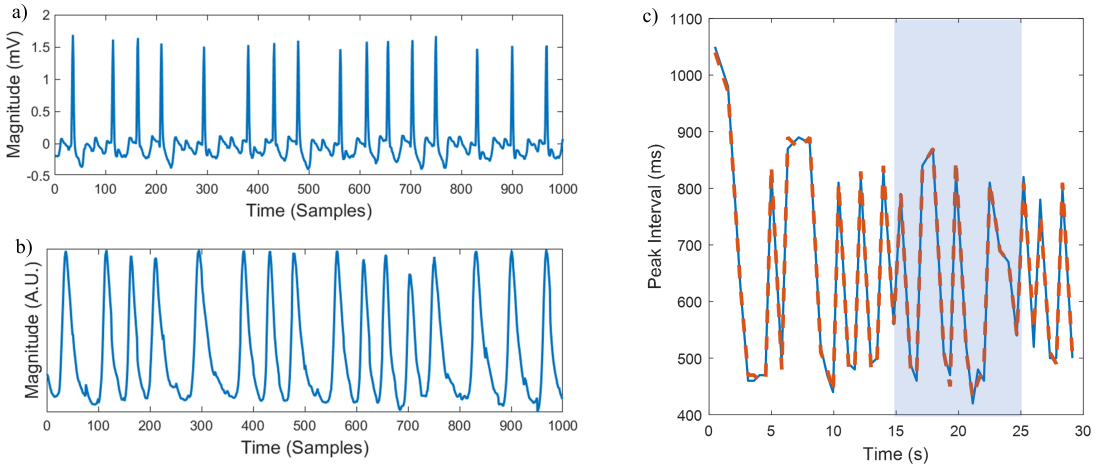

FIGURE 13. a) An example of atrial fibrillation ECG. For better inspection, 10 seconds of the signal is shown out of the 30-second segment. b) GAN generated PPG segment from the input atrial fibrillation ECG shown in a). c) Plot showing ECG RR interval (solid lines) and PPG systolic peak interval (dashed line). The shaded region corresponds to the 10-second segment shown in a) and b). [Note: ECG, electrocardiogram; PPG, photoplethysmogram].

v1.0.0 [75], [76] was used to generate synthetic counterpart PPG. From 84 long-term ECG recordings, 69 recordings annotated as atrial fibrillation were included for this purpose. Afterwards, 13 recordings with ECG too noisy for peak detection were excluded. Finally, test dataset consisting of 280 segments of 30-second atrial fibrillation ECG from 56 patients (5 segments per patient) were used to generated synthetic atrial fibrillation PPG segments after GAN optimization (i.e. none of these 280 segments were used in training). To determine the presence of atrial fibrillation in the generated PPG segments, beat-by-beat heart rates found in the source ECG and the generated PPG were compared, under the assumption that heart rate could be a reliable predictor of atrial fibrillation with sensitivity around 95% [67], [69], [77]. Correlation coefficient between the beat-by-beat heart rate measured across the atrial fibrillation ECG segments and in the corresponding generated PPG segments was 0.94 ± 0.15, and comparison using paired t-test yielded a p-value of 0.64, indicating the highest association with no significant difference between the two as depicted on Fig. 13. These preliminary results indicate that the proposed GAN model could be potentially used for generating atrial fibrillation PPG data using open atrial fibrillation ECG datasets. In this respect, it is likely that the proposed GAN may improve the accuracy of various atrial fibrillation detection algorithms based on PPG data as it can augment dataset used for training these algorithms by generating PPG reflecting inter-beat interval variability of atrial fibrillation ECG. Considering that only beat-by-beat interval was compared to verify the presence of atrial fibrillation, a full study validating alternative properties of atrial fibrillation in the synthetic PPG is warranted.

Furthermore, the proposed GAN model can be implemented beyond ECG and PPG, and can be applied to any related biosignal pairs, implying the possibility of augmenting biosignal databases that is lacking in one biosignal by generating it from another source.

TABLE 2. PRD & pearson correlation coefficient calculated between reference and synthetic ppg based on different gan architectures.

Metric	GAN	WGAN-GP	LSGAN
PRD (%)	31.9	32.1	32.6
CC	0.949	0.949	0.947

[Note: PRD, percent root mean square difference; CC, correlation coefficient; GAN, generative adversarial network; WGAN-GP, Wasserstein GAN with gradient penalty; LSGAN, least squares GAN]

C. PERFORMANCE COMPARISON BETWEEN VARIOUS GAN ARCHITECTURES

In order to test the performance of the proposed method against different GAN architecture, two alternative GAN models including Wasserstein GAN with gradient penalty (WGAN-GP), and least squares GAN (LSGAN) were trained and tested. Wasserstein GAN with gradient penalty provides more stable training of the GAN model using Wasserstein distance as the loss metric to measure the difference between the generated and reference distributions [78]. LSGAN uses least square distance to measure the difference between real and generated signal distributions, which is more stable with respect to gradients as compared to the original GAN model and converges more rapidly than the method using Wasserstein distance [79]. Additional hyperparameters were kept as described in the original studies, and the MSE loss was retained in the loss function across all three GAN architectures. As shown in Table 2, there were no significant differences between the models in terms of PRD and correlation coefficient.

D. LIMITATIONS

PPG may provide noninvasive modes for assessing arterial structure and function [80]–[82]. The morphology of the PPG

signal can be defined in two phases: (1) the rising phase concerned with systole, and (2) the descending phase concerned with diastole and wave reflections from the periphery. A dicrotic notch is prevalent in the descending phase of young subjects with healthy compliant arteries and stiffening of the small arteries alters the magnitude and timing of reflected waves [83], [84]. In this respect, this study has a limitation in generating PPG signals with conditions related to arterial stiffness in that there are no distinctive dicrotic notches in some of the generated PPG. However, it is also noted that the PPG was generated using ECG as the input. Unlike PPG, ECG does not carry any explicit information related to vascularity like the prominence of the dicrotic notch. Since the proposed GAN generates PPG based on ECG, the lack of information on vascularity is inevitable. To overcome such limitations, one can incorporate patients' age and information about their cardiovascular conditions during training of the GAN. By providing extra information related to vascularity into the network, the network might be able to reproduce these information as distinct features in the generated PPG signal.

As mentioned above, there are validating the presence of atrial fibrillation in synthetic PPG using heart rate has a few limitations. First, ECG P-wave which shows the electrical depolarization of atria is unavailable if using PPG-based approach [85], [86]. This hinders other methods of analyzing atrial fibrillation risk using P-wave duration, and morphology. Second, some atrial fibrillation detection based on deep neural networks focus on specific substructures in PPG morphology such as locations of systolic and diastolic peaks, as well as slopes of the curve before the systolic peaks [16], [87]. In this study, however, it is impossible to test the morphological properties of the synthetic atrial fibrillation PPG as there are no reference PPG signals available from the test dataset. In order to assess the performance of the optimized GAN in terms of atrial fibrillation PPG morphology, it is necessary to test the model in a dataset with both ECG and PPG simultaneously recorded from atrial fibrillation patients.

V. CONCLUSION

In this study, a novel GAN-based PPG data augmentation method using ECG is proposed. Our preliminary results indicate that the optimized GAN can generate PPG signals well correlated with reference PPG with low PRD and high correlation coefficient. Furthermore, it can encode beat-by-beat ECG heart rate, and replicate it in the synthetic PPG signal even with the presence of atrial fibrillation. The results of this study indicate that the proposed method has wide applications in biosignal augmentation.

REFERENCES

[1] H. Lee, E. Kim, Y. Lee, H. Kim, J. Lee, M. Kim, H.-J. Yoo, and S. Yoo, "Toward all-day wearable health monitoring: An ultralow-power, reflective organic pulse oximetry sensing patch," *Sci. Adv.*, vol. 4, no. 11, Nov. 2018, Art. no. eaas9530.

[2] D. Son, J. Lee, S. Qiao, R. Ghaffari, J. Kim, J. E. Lee, C. Song, S. J. Kim, D. J. Lee, and S. W. Jun, "Multifunctional wearable devices for diagnosis and therapy of movement disorders," *Nature Nanotechnol.*, vol. 9, no. 5, p. 397, Mar. 2014.

[3] Y.-L. Zheng, X.-R. Ding, C. C. Y. Poon, B. P. L. Lo, H. Zhang, X.-L. Zhou, G.-Z. Yang, N. Zhao, and Y.-T. Zhang, "Unobtrusive sensing and wearable devices for health informatics," *IEEE Trans. Biomed. Eng.*, vol. 61, no. 5, pp. 1538–1554, May 2014.

[4] S. Kwon, J. Hong, E.-K. Choi, B. Lee, C. Baik, E. Lee, E.-R. Jeong, B.-K. Koo, S. Oh, and Y. Yi, "Detection of atrial fibrillation using a ring-type wearable device (CardioTracker) and deep learning analysis of photoplethysmography signals: Prospective observational Proof-of-Concept study," *J. Med. Internet Res.*, vol. 22, no. 5, May 2020, Art. no. e16443.

[5] M. Elgendi, R. Fletcher, Y. Liang, N. Howard, N. H. Lovell, D. Abbott, K. Lim, and R. Ward, "The use of photoplethysmography for assessing hypertension," *npj Digit. Med.*, vol. 2, no. 1, pp. 1–11, Dec. 2019.

[6] H. Xu, J. Liu, J. Zhang, G. Zhou, N. Luo, and N. Zhao, "Flexible organic/inorganic hybrid near-infrared photoplethysmogram sensor for cardiovascular monitoring," *Adv. Mater.*, vol. 29, no. 31, 2017, Art. no. 1700975.

[7] M.-Z. Poh, K. Kim, A. Goessling, N. Swenson, and R. Picard, "Cardiovascular monitoring using earphones and a mobile device," *IEEE Pervas. Comput.*, vol. 11, no. 4, pp. 18–26, Oct. 2012.

[8] Y. Liang, Z. Chen, R. Ward, and M. Elgendi, "Photoplethysmography and deep learning: Enhancing hypertension risk stratification," *Biosensors*, vol. 8, no. 4, p. 101, Oct. 2018.

[9] M. Panwar, A. Gautam, D. Biswas, and A. Acharyya, "PP-Net: A deep learning framework for PPG-based blood pressure and heart rate estimation," *IEEE Sensors J.*, vol. 20, no. 17, pp. 10000–10011, Sep. 2020.

[10] J. M. J. Huttunen, L. Kärkkäinen, M. Honkala, and H. Lindholm, "Deep learning for prediction of cardiac indices from photoplethysmographic waveform: A virtual database approach," *Int. J. Numer. Methods Biomed. Eng.*, vol. 36, no. 3, Mar. 2020, p. e3303.

[11] G. Slapničar, N. Mlakar, and M. Luštrek, "Blood pressure estimation from photoplethysmogram using a spectro-temporal deep neural network," *Sensors*, vol. 19, no. 15, p. 3420, Aug. 2019.

[12] O. Schlesinger, N. Vigderhouse, Y. Moshe, and D. Eytan, "Estimation and tracking of blood pressure using routinely acquired photoplethysmographic signals and deep neural networks," *Crit. Care Explor.*, vol. 2, no. 4, p. e0095, 2020.

[13] D. Biswas, L. Everson, M. Liu, M. Panwar, B.-E. Verhoef, S. Patki, C. H. Kim, A. Acharyya, C. Van Hoof, M. Konijnenburg, and N. Van Helleputte, "CorNET: Deep learning framework for PPG-based heart rate estimation and biometric identification in ambulant environment," *IEEE Trans. Biomed. Circuits Syst.*, vol. 13, no. 2, pp. 282–291, Apr. 2019.

[14] L. Everson, D. Biswas, M. Panwar, D. Rodopoulos, A. Acharyya, C. H. Kim, C. Van Hoof, M. Konijnenburg, and N. Van Helleputte, "BiometricNet: Deep learning based biometric identification using wrist-worn PPG," in *Proc. IEEE Int. Symp. Circuits Syst. (ISCAS)*, May 2018, pp. 1–5.

[15] Y. Shen, M. Voisin, A. Aliamiri, A. Avati, A. Hannun, and A. Ng, "Ambulatory atrial fibrillation monitoring using wearable photoplethysmography with deep learning," in *Proc. 25th ACM SIGKDD Int. Conf. Knowl. Discovery Data Mining*, Jul. 2019, pp. 1909–1916.

[16] S. P. Shashikumar, A. J. Shah, Q. Li, G. D. Clifford, and S. Nemati, "A deep learning approach to monitoring and detecting atrial fibrillation using wearable technology," in *Proc. IEEE EMBS Int. Conf. Biomed. Health Informat. (BHI)*, Feb. 2017, pp. 141–144.

[17] M.-Z. Poh, Y. C. Poh, P.-H. Chan, C.-K. Wong, L. Pun, W. W.-C. Leung, Y.-F. Wong, M. M.-Y. Wong, D. W.-S. Chu, and C.-W. Siu, "Diagnostic assessment of a deep learning system for detecting atrial fibrillation in pulse waveforms," *Heart*, vol. 104, no. 23, pp. 1921–1928, Dec. 2018.

[18] S. Kwon, J. Hong, E.-K. Choi, E. Lee, D. E. Hostallero, W. J. Kang, B. Lee, E.-R. Jeong, B.-K. Koo, S. Oh, and Y. Yi, "Deep learning approaches to detect atrial fibrillation using photoplethysmographic signals: Algorithms development study," *JMIR mHealth uHealth*, vol. 7, no. 6, Jun. 2019, Art. no. e12770.

[19] Y. Liang, Z. Chen, R. Ward, and M. Elgendi, "Hypertension assessment via ECG and PPG signals: An evaluation using MIMIC database," *Diagnostics*, vol. 8, no. 3, p. 65, Sep. 2018.

[20] Y. Zhang and Z. Feng, "A SVM method for continuous blood pressure estimation from a PPG signal," in *Proc. 9th Int. Conf. Mach. Learn. Comput.*, Feb. 2017, pp. 128–132.

[21] A. Reiss, I. Indlekofer, P. Schmidt, and K. Van Laerhoven, "Deep PPG: Large-scale heart rate estimation with convolutional neural networks," *Sensors*, vol. 19, no. 14, p. 3079, Jul. 2019.
[22] K. Aschbacher, D. Yilmaz, Y. Kerem, S. Crawford, D. Benaron, J. Liu, M. Eaton, G. H. Tison, J. E. Olgin, Y. Li, and G. M. Marcus, "Atrial fibrillation detection from raw photoplethysmography waveforms: A deep learning application," *Heart Rhythm O2*, vol. 1, no. 1, pp. 3–9, Apr. 2020.
[23] A. Aliamiri and Y. Shen, "Deep learning based atrial fibrillation detection using wearable photoplethysmography sensor," in *Proc. IEEE EMBS Int. Conf. Biomed. Health Inform. (BHI)*, Mar. 2018, pp. 442–445.
[24] P. Kostkova, H. Brewer, S. de Lusignan, E. Fottrell, B. Goldacre, G. Hart, P. Koczan, P. Knight, C. Marsolier, R. A. McKendry, E. Ross, A. Sasse, R. Sullivan, S. Chaytor, O. Stevenson, R. Velho, and J. Tooke, "Who owns the data? Open data for healthcare," *Frontiers Public Health*, vol. 4, p. 7, Feb. 2016.
[25] P. Warrick and M. Nabhan Homsi, "Cardiac arrhythmia detection from ECG combining convolutional and long short-term memory networks," in *Proc. Comput. Cardiol. Conf. (CinC)*, Sep. 2017, pp. 1–4.
[26] A. Sološenko, A. Petrėnas, V. Marozas, and L. Sörnmo, "Modeling of the photoplethysmogram during atrial fibrillation," *Comput. Biol. Med.*, vol. 81, pp. 130–138, Feb. 2017.
[27] F. Zhu, F. Ye, Y. Fu, Q. Liu, and B. Shen, "Electrocardiogram generation with a bidirectional LSTM-CNN generative adversarial network," *Sci. Rep.*, vol. 9, no. 1, pp. 1–11, Dec. 2019.
[28] K. Gregor Hartmann, R. Tibor Schirrmeister, and T. Ball, "EEG-GAN: Generative adversarial networks for electroencephalograhic (EEG) brain signals," 2018, *arXiv:1806.01875*. [Online]. Available: http://arxiv.org/abs/1806.01875
[29] E. Brophy, Z. Wang, and T. E. Ward, "Quick and easy time series generation with established image-based GANs," 2019, *arXiv:1902.05624*. [Online]. Available: http://arxiv.org/abs/1902.05624
[30] T. Golany and K. Radinsky, "PGANS: Personalized generative adversarial networks for ECG synthesis to improve patient-specific deep ECG classification," in *Proc. AAAI Conf. Artif. Intell.*, vol. 33, 2019, pp. 557–564.
[31] T. Golany, K. Radinsky, and D. Freedman, "SimGANs: Simulator-based generative adversarial networks for ECG synthesis to improve deep ECG classification," in *Proc. Int. Conf. Mach. Learn.*, 2020, pp. 3597–3606.
[32] D. Hazra and Y.-C. Byun, "SynSigGAN: Generative adversarial networks for synthetic biomedical signal generation," *Biology*, vol. 9, no. 12, p. 441, Dec. 2020.
[33] I. Goodfellow, "Generative adversarial nets," in *Proc. Adv. Neural Inf. Process. Syst.*, 2014, pp. 2672–2680.
[34] J.-Y. Zhu, T. Park, P. Isola, and A. A. Efros, "Unpaired image-to-image translation using cycle-consistent adversarial networks," in *Proc. IEEE Int. Conf. Comput. Vis. (ICCV)*, Oct. 2017, pp. 2223–2232.
[35] D. Kiyasseh, G. A. Tadesse, L. N. T. Nhan, L. Van Tan, L. Thwaites, T. Zhu, and D. Clifton, "PlethAugment: GAN-based PPG augmentation for medical diagnosis in low-resource settings," *IEEE J. Biomed. Health Informat.*, vol. 24, no. 11, pp. 3226–3235, Nov. 2020.
[36] C. Esteban, S. L. Hyland, and G. Rätsch, "Real-valued (Medical) time series generation with recurrent conditional GANs," 2017, *arXiv:1706.02633*. [Online]. Available: http://arxiv.org/abs/1706.02633
[37] H.-C. Lee and C.-W. Jung, "Vital Recorder—A free research tool for automatic recording of high-resolution time-synchronised physiological data from multiple anaesthesia devices," *Sci. Rep.*, vol. 8, no. 1, p. 1527, 2018.
[38] S. Hochreiter and J. Schmidhuber, "Long short-term memory," *Neural Comput.*, vol. 9, no. 8, pp. 1735–1780, 1997.
[39] D. Liu, M. Görges, and S. A. Jenkins, "University of Queensland vital signs dataset: Development of an accessible repository of anesthesia patient monitoring data for research," *Anesthesia Analgesia*, vol. 114, no. 3, pp. 584–589, 2012.
[40] K. Abouelmehdi, A. Beni-Hessane, and H. Khaloufi, "Big healthcare data: Preserving security and privacy," *J. Big Data*, vol. 5, no. 1, p. 1, Dec. 2018.
[41] D. Ravì, C. Wong, and F. Deligianni, "Deep learning for health informatics," *IEEE J. Biomed. Health Inform.*, vol. 21, no. 1, pp. 4–21, Jan. 2017.
[42] K. Nikolaidis, S. Kristiansen, V. Goebel, T. Plagemann, K. Liestøl, and M. Kankanhalli, "Augmenting physiological time series data: A case study for sleep apnea detection," in *Proc. Joint Eur. Conf. Mach. Learn. Knowl. Discovery Databases*. Cham, Switzerland: Springer, 2019, pp. 376–399.
[43] W. B. Murray and P. A. Foster, "The peripheral pulse wave: Information overlooked," *J. Clin. Monitor.*, vol. 12, no. 5, pp. 365–377, Sep. 1996.
[44] J. Allen and A. Murray, "Age-related changes in the characteristics of the photoplethysmographic pulse shape at various body sites," *Physiol. Meas.*, vol. 24, no. 2, p. 297, 2003.
[45] A. Maheshwari, F. L. Norby, E. Z. Soliman, S. Adabag, E. A. Whitsel, A. Alonso, and L. Y. Chen, "Low heart rate variability in a 2-minute electrocardiogram recording is associated with an increased risk of sudden cardiac death in the general population: The atherosclerosis risk in communities study," *PLoS ONE*, vol. 11, no. 8, Aug. 2016, Art. no. e0161648.
[46] F. Sessa, V. Anna, G. Messina, G. Cibelli, and V. Monda, "Heart rate variability as predictive factor for sudden cardiac death," *Aging (Albany NY)*, vol. 10, no. 2, p. 166, 2018.
[47] I. Saito, Y. Takata, K. Maruyama, E. Eguchi, T. Kato, R. Shirahama, K. Tomooka, R. Kawamura, M. Sano, Y. Tabara, H. Osawa, and T. Tanigawa, "Association between heart rate variability and home blood pressure: The toon health study," *Amer. J. Hypertension*, vol. 31, no. 10, pp. 1120–1126, Sep. 2018.
[48] K. Trimmel, J. Sacha, and H. V. Huikuri, *Heart Rate Variability: Clinical Applications and Interaction Between HRV and Heart Rate*. Lausanne, Switzerland: Frontiers Media SA, 2015.
[49] A. Günther, O. Witte, and D. Hoyer, "Autonomic dysfunction and risk stratification assessed from heart rate pattern," *Open Neurol. J.*, vol. 4, p. 39, May 2010.
[50] H. Yoon, S. H. Hwang, J.-W. Choi, Y. J. Lee, D.-U. Jeong, and K. S. Park, "REM sleep estimation based on autonomic dynamics using R–R intervals," *Physiol. Meas.*, vol. 38, no. 4, p. 631, 2017.
[51] J. Hayano, N. Ueda, M. Kisohara, Y. Yoshida, H. Tanaka, and E. Yuda, "Non-REM sleep marker for wearable monitoring: Power concentration of respiratory heart rate fluctuation," *Appl. Sci.*, vol. 10, no. 9, p. 3336, May 2020.
[52] W. Jung, K.-I. Jang, and S.-H. Lee, "Heart and brain interaction of psychiatric illness: A review focused on heart rate variability, cognitive function, and quantitative electroencephalography," *Clin. Psychopharmacol. Neurosci.*, vol. 17, no. 4, p. 459, 2019.
[53] ELECTROPHYSIOLOGY, Task Force of the European Society of Cardiology the North American Society of Pacing, "Heart rate variability: Standards of measurement, physiological interpretation, and clinical use," *Circulation*, vol. 93, no. 5, pp. 1043–1065, 1996.
[54] G. A. Lanza, "Prognostic value of ventricular arrhythmias and heart rate variability in patients with unstable angina," *Heart*, vol. 92, no. 8, pp. 1055–1063, Aug. 2006.
[55] G. Liu, L. Wang, Q. Wang, G. Zhou, Y. Wang, and Q. Jiang, "A new approach to detect congestive heart failure using short-term heart rate variability measures," *PLoS ONE*, vol. 9, no. 4, Apr. 2014, Art. no. e93399.
[56] W. Hu, X. Jin, P. Zhang, Q. Yu, G. Yin, Y. Lu, H. Xiao, Y. Chen, and D. Zhang, "Deceleration and acceleration capacities of heart rate associated with heart failure with high discriminating performance," *Sci. Rep.*, vol. 6, no. 1, pp. 1–10, Apr. 2016.
[57] A. A. Khan, G. Y. H. Lip, and A. Shantsila, "Heart rate variability in atrial fibrillation: The balance between sympathetic and parasympathetic nervous system," *Eur. J. Clin. Invest.*, vol. 49, no. 11, Nov. 2019.
[58] A. Bauer, J. W. Kantelhardt, P. Barthel, R. Schneider, T. Mäkikallio, K. Ulm, K. Hnatkova, A. Schömig, H. Huikuri, A. Bunde, M. Malik, and G. Schmidt, "Deceleration capacity of heart rate as a predictor of mortality after myocardial infarction: Cohort study," *Lancet*, vol. 367, no. 9523, pp. 1674–1681, May 2006.
[59] K. D. Rizas, C. Eick, A. J. Doller, W. Hamm, L. von Stuelpnagel, C. S. Zuern, P. Barthel, G. Schmidt, and A. Bauer, "Bedside autonomic risk stratification after myocardial infarction by means of short-term deceleration capacity of heart rate," *EP Europace*, vol. 20, no. FI1, pp. f129–f136, Jun. 2018.
[60] X.-D. Wang, L. Zhou, C.-Y. Zhu, B. Chen, Z. Chen, and L. Wei, "Autonomic function as indicated by heart rate deceleration capacity and deceleration runs in type 2 diabetes patients with or without essential hypertension," *Clin. Interventions Aging*, vol. 13, p. 1169, Aug. 2018.
[61] T. Benichou, B. Pereira, M. Mermillod, P. Daniela, I. Tauveron, S. Maqdasy, and F. Dutheil, "Heart rate variability in type 2 diabetes mellitus: A systematic review and meta-analysis," *Annales d'Endocrinologie*, vol. 79, no. 4, pp. 465–466, Sep. 2018.
[62] S. Lu, H. Zhao, K. Ju, K. Shin, M. Lee, K. Shelley, and K. H. Chon, "Can photoplethysmography variability serve as an alternative approach to obtain heart rate variability information?" *J. Clin. Monitor. Comput.*, vol. 22, no. 1, pp. 23–29, Jan. 2008.
[63] C. Gutierrez and D. G. Blanchard, "Diagnosis and treatment of atrial fibrillation," *Amer. Family Physician*, vol. 94, no. 6, pp. 442–452, 2016.

[64] J. Kornej, C. S. Börschel, E. J. Benjamin, and R. B. Schnabel, "Epidemiology of atrial fibrillation in the 21st century: Novel methods and new insights," *Circulat. Res.*, vol. 127, no. 1, pp. 4–20, 2020.
[65] H. Dai, Q. Zhang, A. A. Much, and E. Maor, "Global, regional, and national prevalence, incidence, mortality, and risk factors for atrial fibrillation, 1990–2017: Results from the Global Burden of disease study 2017," *Eur. Heart J.-Qual. Care Clin. Outcomes*, pp. 1–9, 2020.
[66] X. Cui, E. Chang, W.-H. Yang, B. Jiang, A. Yang, and C.-K. Peng, "Automated detection of paroxysmal atrial fibrillation using an information-based similarity approach," *Entropy*, vol. 19, no. 12, p. 677, Dec. 2017.
[67] J. Lian, L. Wang, and D. Muessig, "A simple method to detect atrial fibrillation using RR intervals," *Amer. J. Cardiol.*, vol. 107, no. 10, pp. 1494–1497, May 2011.
[68] R. Czabanski, K. Horoba, J. Wrobel, A. Matonia, R. Martinek, T. Kupka, M. Jezewski, R. Kahankova, J. Jezewski, and J. Leski, "Detection of atrial fibrillation episodes in long-term heart rhythm signals using a support vector machine," *Sensors*, vol. 20, no. 3, p. 765, Jan. 2020.
[69] J. Park, S. Lee, and M. Jeon, "Atrial fibrillation detection by heart rate variability in poincare plot," *Biomed. Eng. OnLine*, vol. 8, no. 1, p. 38, 2009.
[70] L. M. Eerikäinen, A. G. Bonomi, F. Schipper, L. R. C. Dekker, R. Vullings, H. M. de Morree, and R. M. Aarts, "Comparison between electrocardiogram-and photoplethysmogram-derived features for atrial fibrillation detection in free-living conditions," *Physiol. Meas.*, vol. 39, no. 8, 2018, Art. no. 084001.
[71] S. Nemati, M. M. Ghassemi, V. Ambai, N. Isakadze, O. Levantsevych, A. Shah, and G. D. Clifford, "Monitoring and detecting atrial fibrillation using wearable technology," in *Proc. 38th Annu. Int. Conf. IEEE Eng. Med. Biol. Soc. (EMBC)*, Aug. 2016, pp. 3394–3397.
[72] A. G. Bonomi, F. Schipper, L. M. Eerikäinen, J. Margarito, R. M. Aarts, S. Babaeizadeh, H. M. de Morree, and L. Dekker, "Atrial fibrillation detection using photo-plethysmography and acceleration data at the wrist," in *Proc. Comput. Cardiol. Conf. (CinC)*, Sep. 2016, pp. 277–280.
[73] J. W. Chong, N. Esa, D. D. McManus, and K. H. Chon, "Arrhythmia discrimination using a smart phone," *IEEE J. Biomed. Health Inform.*, vol. 19, no. 3, pp. 815–824, May 2015.
[74] S. K. Bashar, D. Han, S. Hajeb-Mohammadalipour, E. Ding, C. Whitcomb, D. D. Mcmanus, and K. H. Chon, "Atrial fibrillation detection from wrist photoplethysmography signals using smartwatches," *Sci. Rep.*, vol. 9, no. 1, pp. 1–10, Dec. 2019.
[75] S. Petrutiu, A. V. Sahakian, and S. Swiryn, "Abrupt changes in fibrillatory wave characteristics at the termination of paroxysmal atrial fibrillation in humans," *EP Europace*, vol. 9, no. 7, pp. 466–470, Jul. 2007.
[76] A. L. Goldberger, L. A. N. Amaral, L. Glass, and J. M. Hausdorff, "PhysioBank, PhysioToolkit, and PhysioNet: Components of a new research resource for complex physiologic signals," *Circulation*, vol. 101, no. 23, pp. e215–e220, 2000.
[77] D. D. Mcmanus, J. Lee, O. Maitas, N. Esa, R. Pidikiti, A. Carlucci, J. Harrington, E. Mick, and K. H. Chon, "A novel application for the detection of an irregular pulse using an iPhone 4S in patients with atrial fibrillation," *Heart Rhythm*, vol. 10, no. 3, pp. 315–319, Mar. 2013.
[78] I. Gulrajani, F. Ahmed, M. Arjovsky, V. Dumoulin, and A. C. Courville, "Improved training of Wasserstein GANs," in *Proc. Adv. Neural Inf. Process. Syst.*, 2017, pp. 5767–5777.
[79] X. Mao, Q. Li, H. Xie, R. Y. K. Lau, Z. Wang, and S. P. Smolley, "Least squares generative adversarial networks," in *Proc. IEEE Int. Conf. Comput. Vis. (ICCV)*, Oct. 2017, pp. 2794–2802.
[80] S. C. Millasseau, J. M. Ritter, K. Takazawa, and P. J. Chowienczyk, "Contour analysis of the photoplethysmographic pulse measured at the finger," *J. Hypertension*, vol. 24, no. 8, pp. 1449–1456, 2006.
[81] L. A. Bortolotto, J. Blacher, T. Kondo, K. Takazawa, and M. E. Safar, "Assessment of vascular aging and atherosclerosis in hypertensive subjects: Second derivative of photoplethysmogram versus pulse wave velocity," *Amer. J. Hypertension*, vol. 13, no. 2, pp. 165–171, Feb. 2000.
[82] D. N. Dutt and S. Shruthi, "Digital processing of ECG and PPG signals for study of arterial parameters for cardiovascular risk assessment," in *Proc. Int. Conf. Commun. Signal Process. (ICCSP)*, Apr. 2015, pp. 1506–1510.
[83] P. Shi, S. Hu, Y. Zhu, J. Zheng, Y. Qiu, and P. Y. S. Cheang, "Insight into the dicrotic notch in photoplethysmographic pulses from the finger tip of young adults," *J. Med. Eng. Technol.*, vol. 33, no. 8, pp. 628–633, Nov. 2009.
[84] M. Elgendi, "On the analysis of fingertip photoplethysmogram signals," *Current Cardiol. Rev.*, vol. 8, no. 1, pp. 14–25, Jun. 2012.
[85] E. Y. Ding, G. M. Marcus, and D. D. Mcmanus, "Emerging technologies for identifying atrial fibrillation," *Circulat. Res.*, vol. 127, no. 1, pp. 128–142, Jun. 2020.
[86] J. Harju, A. Tarniceriu, J. Parak, A. Vehkaoja, A. Yli-Hankala, and I. Korhonen, "Monitoring of heart rate and inter-beat intervals with wrist plethysmography in patients with atrial fibrillation," *Physiol. Meas.*, vol. 39, no. 6, Jun. 2018, Art. no. 065007.
[87] S. Snigdha Sarathi Das, S. Karmaker Shanto, M. Rahman, M. Saiful Islam, A. Rahman, M. Mehedy Masud, and M. Eunus Ali, "BayesBeat: A Bayesian deep learning approach for atrial fibrillation detection from noisy photoplethysmography data," 2020, *arXiv:2011.00753*. [Online]. Available: http://arxiv.org/abs/2011.00753

HEEAN SHIN was born in South Korea, in 1990. She received the B.S. degree from Chung Ang University, Seoul, South Korea, in 2015. She is currently pursuing the Ph.D. degree in biosignal processing with Seoul National University. Her research interests include deep learning-based biosignal processing and artificial organs.

SUKKYU SUN was born in South Korea, in 1991. He received the B.S. degree from the Korea Advanced Institute of Science and Technology (KAIST), Daejeon, South Korea, in 2014, the M.S. degree from Seoul National University, South Korea, in 2016, and the interdisciplinary Ph.D. degree in bioengineering from the Seoul National University Graduate School, Seoul, South Korea, in 2021. He is currently a Research Professor with the Biomedical Research Institute, Seoul National University Hospital. His research interest includes deep learning-based imaging.

JOONNYONG LEE received the B.A. degree in mathematics, and the B.S. and M.Eng. degrees in biomedical engineering from Boston University. He is currently the Founder and the CEO of Mellowing Factory Company Ltd., which develops electronics for sleep quality improvement. His research interests include deep learning-based biosignal processing methods, health informatics, and ubiquitous healthcare. His Ph.D. dissertation at Seoul National University was on biosignal processing using recurrent neural networks, in 2019.

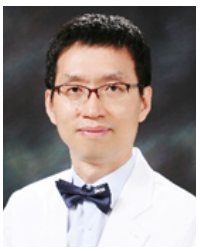

HEE CHAN KIM (Member, IEEE) received the Ph.D. degree in control and instrumentation engineering (biomedical engineering) from Seoul National University, Seoul, South Korea, in 1989. From 1989 to 1991, he was a Staff Engineer working with the National Institute of Health(NIH)-funded Electrohydraulic Total Artificial Heart Project at the Artificial Heart Research Laboratory, The University of Utah, Salt Lake City, USA. He joined the Faculty of the Department of Biomedical Engineering, College of Medicine, Seoul National University and Seoul National University Hospital, in 1991, where he is currently a Professor with the Medical Electronics Laboratory(MELab). His research interests include development of intelligent algorithms and electronic instrumentations for medical and biological applications including artificial organs, such as artificial heart and artificial pancreas, biosensors, ubiquitous/mobile healthcare systems, and man-machine interface. In these areas, he has published over 210 peer-reviewed scientific articles in international journals and holds more than 170 patents. He is a member of the Korea Society of Medical and Biological Engineering (KOSOMBE), IEEE/EMBS, and the American Society of Artificial Internal Organs (ASAIO).